UPPSALA
UNIVERSITET

Digital Comprehensive Summaries of Uppsala Dissertations from the Faculty of Science and Technology 1029

Measurement and modelling of unbalanced magnetic pull in hydropower generators

MATTIAS WALLIN

ACTA
UNIVERSITATIS
UPSALIENSIS
UPPSALA
2013

ISSN 1651-6214
ISBN 978-91-554-8619-8
urn:nbn:se:uu:diva-196490

Dissertation presented at Uppsala University to be publicly examined in Polhemssalen, Ångström Laboratory, Lägerhyddsvägen 1, Uppsala, Friday, April 26, 2013 at 13:15 for the degree of Doctor of Philosophy. The examination will be conducted in English.

Abstract
Wallin, M. 2013. Measurement and modelling of unbalanced magnetic pull in hydropower generators. Acta Universitatis Upsaliensis. *Digital Comprehensive Summaries of Uppsala Dissertations from the Faculty of Science and Technology* 1029. 51 pp. Uppsala. ISBN 978-91-554-8619-8.

Hydropower research is often perceived to be an old and exhausted field of study but with ageing equipment and the need for more intermittent operation caused by an increased share of other renewable energy sources new challenges lie ahead.

The main focus of this dissertation are the electromagnetic forces resulting from nonuniform air gap flux, whether it be caused by rotor eccentricity or a faulty field winding. Results are predominantly obtained from measurements on an experimental generator and numerical simulations.

With the computational capacity available today it is possible to numerically analyse physical phenomena that previously could only be studied with analytical tools. Numerical models can also be expanded to encompass more than one aspect of generator operation in coupled field-circuit models without model complexity surpassing computer capability.

Three studies of unbalanced magnetic pull, UMP, in synchronous salient pole generators constitute the main part of this thesis.

The first is a study of how parallel stator circuits affect the unbalanced magnetic pull caused by rotor eccentricity. Depending on the relationship between the geometry of the separate circuits and the direction of the eccentricity it was found that parallel circuits could reduce the UMP substantially.

Secondly, an investigation of the effect of damper winding configuration on UMP was performed. The results showed that damper winding resistivity and the distance between the damper bars in a pole determine the effectiveness of the damper winding in reducing the UMP. Simulations of a production machine indicate that the reduction can be substantial from damper windings with low resistivity.

The third study analyses the consequences of field winding interturn short circuits. Apart from a resulting rotating unbalanced magnetic pull it is found that the unaffected poles with the same polarity as the affected pole experience an increase in flux density.

In a fourth article a new stand still frequency response, SSFR, test method including measurements of damper winding voltage and current is presented. It is found that the identified models are capable of predicting the stator to damper transfer function both with and without the damper winding measurements included.

Keywords: Damper winding, eddy currents, field winding short circuit, finite element method, hydropower generator, parallel circuits, rotor eccentricity, salient poles, synchronous generators, synchronous machines, UMP, unbalanced magnetic pull.

Mattias Wallin, Uppsala University, Department of Engineering Sciences, Electricity, Box 534, SE-751 21 Uppsala, Sweden.

ISSN 1651-6214
ISBN 978-91-554-8619-8
urn:nbn:se:uu:diva-196490 (http://urn.kb.se/resolve?urn=urn:nbn:se:uu:diva-196490)

Till Ann

List of papers

This thesis is based on the following papers, which are referred to in the text by their roman numerals.

I **Wallin**, **M.**, Ranlöf M. and Lundin U., ”Design and construction of a synchronous generator test setup”, *XIX International Conference on Electrical Machines*, September 2010.

II **Wallin**, **M.**, Ranlöf, M. and Lundin, U., ”Reduction of unbalanced magnetic pull in synchronous machines due to parallel circuits”, *IEEE Transactions on Magnetics*, vol. 47, no. 12, pp. 4827-4833, 2011.

III **Wallin**, **M.**, Bladh, J. and Lundin, U., ”Damper winding influence on unbalanced magnetic pull in synchronous machines with rotor eccentricity”, *submitted to IEEE Transactions on Magnetics*, November 2012.

IV **Wallin**, **M.**, and Lundin, U., ”Dynamic unbalanced pull from field winding turn short circuit”, *submitted to Electric Power Components and Systems*, February 2013.

V Bladh, J., **Wallin**, **M.**, Saarinen, L. and Lundin, U., ”Stand-still frequency response test including damper winding measurements”, unpublished manuscript.

Contents

1 Introduction 1
- 1.1 Hydropower in a new light 1
- 1.2 Project background 1
- 1.3 Content of the thesis 2

2 Synchronous generators 3
- 2.1 Rotor 3
- 2.2 Stator 5
- 2.3 Magnetic circuit equivalent 5

3 Eccentricity 7
- 3.1 Permeance 8
- 3.2 Unbalanced magnetic pull 9

4 Finite element analysis 11
- 4.1 The field-circuit problem 11
- 4.2 Geometry 12
- 4.3 Solutions 14

5 Research areas 15
- 5.1 Parallel circuits and rotor eccentricity 15
- 5.2 Damper windings and rotor eccentricity 17
- 5.3 Field winding interturn short circuit 19
- 5.4 Standstill frequency response test 20

6 Experimental generator 21
- 6.1 Construction 21
- 6.2 Measurements 27

7 Results 31
- 7.1 Magnetic saturation 31
- 7.2 Parallel circuits and rotor eccentricity 31
- 7.3 Damper windings and rotor eccentricity 34
- 7.4 Field winding interturn short circuit 35
- 7.5 Results not included in the articles 37

8 Summary of articles 43

9 Svensk sammanfatting 47

10 Acknowledgements 49

Bibliography 51

Nomenclature

Acronyms

Acronym	Description
C	Continuous damper winding
D13-C	Continuous damper winding with bars 1 and 3
D13-NC	Noncontinuous damper winding with bars 1 and 3
D2-C	Continuous damper winding with bar 2
FE	Finite element
FEM	Finite element method
LAN	Local area network
MMF	Magnetomotive force
NC	Noncontinuous damper winding
PC	Parallel circuits
SSFR	Standstill frequency response
THD	Total harmonic distortion
UMP	Unbalanced magnetic pull
WD	Without damper winding
WLAN	Wireless local area network

Greek symbols

Symbol	**Unit**	**Description**
δ	m	Air gap length
ϵ	-	Relative eccentricity
μ_0	Vs/Am	Permeability of empty space
μ_r	-	Relative permeability
Ω	rad	Mechanical frequency
Φ	Wb	Magnetic flux
σ	N/m^2	Stress
τ_s	m	Stator slot pitch
θ	rad	Angular air gap position

Latin symbols

Symbol	Unit	Description
a, b, c	-	Electrical phases
$\mathbf{A}$	Wb/m	Magnetic vector potential
A_z	Wb/m	z-component of the magnetic vector potential
B_n	T	Normal component of the magnetic flux density
B_t	T	Tangential component of the magnetic flux density
d	m	Rotor displacement
F_r	N	Radial force
F_t	N	Tangential force
I	A	Current
I_f	A	Field current
M_f	At	Field winding magnetomotive force
$\mathcal{M}_i$	At	Pole magnetomotive force
N	-	Neutral point in a three phase Y winding
$\mathfrak{R}_g$	A/Wb	Air gap reluctance
$\mathfrak{R}_r$	A/Wb	Rotor reluctance
R_r	m	Rotor radius
$\mathfrak{R}_s$	A/Wb	Stator reluctance
T_m	Nm	Mechanical torque
S_r	m	Stator radius
V	V	Voltage

1. Introduction

In 1878 Aristide Bergès called hydroelectric power the white coal, Fr. *la houille blanche*, to communicate the abundance and availability of the energy stored in the ice and snow of the French Alps.

Hydropower on an industrial scale in Sweden started in 1910 with the commissioning of the first four generators of the Olidan station in Göta Älv in the south west of Sweden. The first large hydropower station in northern Sweden, Porjus, started to deliver electricity in 1915.

Until the introduction of nuclear power to the Swedish electricity production in the seventies and eighties hydropower accounted for the majority of the electricity used in Sweden. It was, and still is, vital to the Swedish welfare and industry. Today hydropower accounts for 45 percent, or 65 TWh, of the electricity used in Sweden.[1]

1.1 Hydropower in a new light

Even though the technology is mature a greater understanding of hydropower generators is needed to avoid failures and undue shortening of the expected service life of the machines. Malfunctioning hydropower generators can lead both to uncertainty in the electricity supply and to increased electricity prices, affecting both households and industries negatively.

Beside the economic impact of nonoperating generators there are environmental gains to make from a high degree of utilisation of our existing hydropower stations.

It is also possible to study electrical machines in new ways due to the computational power available today. Simulations of more complex models where finite element magnetic field simulations are integrated with models of the generator's electric circuits, mechanical properties and thermal characteristics has resulted in more accurate representations of the generators.

1.2 Project background

Unbalanced magnetic pull, UMP, occurs when the rotor is not perfectly centered in the stator or the magnetic flux density in the air gap of a generator is not rotationally symmetric due to some other cause.

[1] A third of the energy used in Sweden is in the form of electricity [1].

UMP can shorten service life and cause failure through increased wear on bearings and other support structures of the rotor and the stator. Asymmetric air gap flux also induces damper winding and intrastator currents which give rise to increased resistive losses and a higher rate of thermal ageing. This thesis investigates three aspects of unbalanced magnetic pull in hydropower generators: how parallel stator circuits can reduce UMP caused by rotor eccentricity, the effects of damper windings under rotor eccentricity and field winding interturn short circuits as a cause of UMP

The work on which the thesis is based has been carried out at the Division of electricity at Uppsala University. Results have been obtained from numerical simulations, analytical models and measurements on the experimental generator built by the author. The generator was named Svante after the donor of the motor upon which the experimental generator was built.

The research presented in this thesis is part of an Elektra programme called *Development of electromagnetic load models for simulation of hydropower rotor-generator systems*. Elektra's sponsors are ABB, the Swedish Transport Administration (Trafikverket), Swedish National Grid (Svenska Kraftnät) and, through Swedenergy (Svensk energi), several electricity production and transmission companies. Elektra's aim is to improve the competitiveness of the Swedish industry through increased research collaboration between universities and the industry.

1.3 Content of the thesis

In the first chapter after the introduction some synchronous generator basics are presented. Chapter 3 explains the geometry of rotor eccentricity. In chapter 4, comes a description of the finite element method, FEM, used in the numerical simulations. After that follows a chapter describing the four research areas: parallel circuits and rotor eccentricity, damper windings and rotor eccentricity, field winding interturn short circuits and a standstill frequency response testing. Chapter 6 describes the mechanical construction considerations behind the design of the experimental generator. Information about the installed sensors and available measurements signals is also presented. Results are presented in chapter 7. The dissertation ends with a brief summary of the included articles.

2. Synchronous generators

This chapter is an introduction to synchronous generators. It also contains some terminology used in the remainder of the thesis and the articles.

Electricity can be generated in several ways, for instance chemically in batteries and fuel cells, through the photovoltaic effect in solar cells or from electromagnetic induction in generators. The most common type of generators are rotating synchronous generators. Focus is placed on salient pole synchronous generators since these are the most common hydroelectric generators but much of the material is applicable to round rotor generators as well as synchronous motors.

At the most basic level hydropower generators convert the potential energy stored in a body of water to electrical energy through the intermediate step of rotating mechanical energy. The torque on the turbine shaft caused by the pressure or kinetic energy of the water drives the rotor shown in figure 2.1. The rotating magnetic field from the field winding on the rotor induces a voltage in the stator winding which in turn will drive a current through any load connected to the generator. Below follows a description of the most important components of a hydropower generator. The names and positions of some generator components are shown in figure 2.1.

2.1 Rotor

A shaft usually connects the turbine runner directly to the rotor and the whole assembly is supported by one thrust and two or more radial fluid film bearings. The mass of the rotating components, excluding the force from the water, can be in excess of 1000 tonnes on a large generator. This rotating mass contributes to the inertia and frequency stability of the grid.

Rotor material

To minimise eddy currents from oscillatory transients and stator slot ripple the entire rotor, apart from the shaft, is made of laminated steel. Electrical sheet steel with a high relative permeability is used to maximise the flux for a given field current.

Field winding

Electromagnetic induction requires a conducting loop and a time magnetic field. On wound field, as opposed to permanent magnet, machines it is the field winding which generates the magnetic flux required to create the generator voltage. The field windings of the separate poles are often connected in series. At every other pole the field winding changes direction around the pole body so the pole fluxes alternate between positive and negative or north and south.

An increase in either the number of field winding turns or the field current increases the air gap flux density, B_δ, and hence the total flux that generates the stator voltage. The current density and resistive losses, i.e. heat generation, in the field winding puts an upper limit on the field current. Magnetic saturation of the rotor and stator steel in combination with the upper limit of the field current governs the stator voltage obtainable.

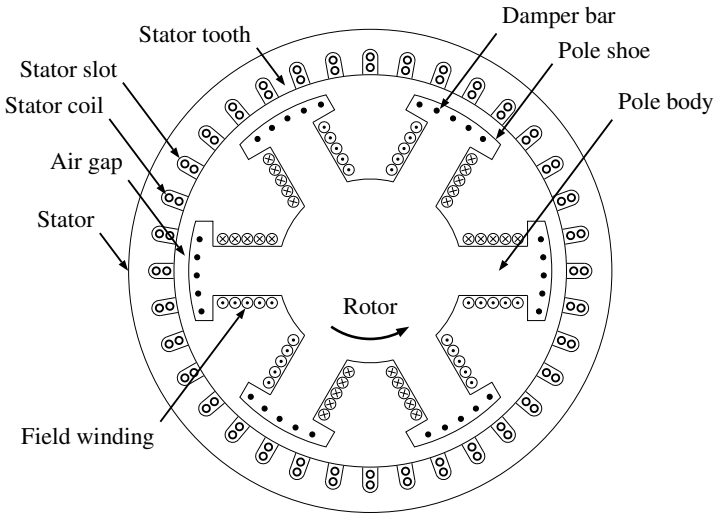

Figure 2.1. A schematic drawing of a wound field synchronous generator with six poles.

Damper winding

Damper windings are axially oriented metal bars, usually copper, placed close to the air gap in the pole shoes of synchronous generators used to dampen oscillatory, electrical or mechanical, transients and to reduce the associated asynchronous air gap flux. Two forms of damper winding connections are common. In the first configurations only the damper bars within a pole are connected and the only path for any interpole damper currents are through the contact between the damper bars and the iron components of the rotor. The

other alternative is a continuous damper winding where the damper bars of each pole are directly connected to the bars of the adjacent poles.

Voltages are induced in the damper bars not only from transients but also due to the stator slots during steady state operation. Losses in the damper bars from stator slot ripple are reduced by keeping the damper slot pitch close to the stator slot pitch, τ_s [2].

To minimise stator voltage harmonics and problems they can cause on the power grid, the damper bars can be tangentially displaced relative to the centre line of the pole, alternating the directions of displacement [3]. Asymmetrically positioned damper bars can be seen in figure 2.1. A shift of the entire pole, instead of just the damper bars, is another common method. Contrary to damper losses stator harmonics can also be reduced by keeping the damper slot pitch close to $0.8\tau_s$ [2].

The effects of damper windings on UMP and the currents induced in the damper winding from rotor eccentricity are studied in III .

2.2 Stator

Together with the air gap and the rotor the stator forms the magnetic circuit of the generator. Electrical sheet steel with a high permeance is used to maximise the flux in the stator core. The flux in the stator changes direction with the electrical frequency and the steel is laminated, usually at a thickness of 0.5 or 0.35 millimetres, to minimise eddy currents.

The alternating flux and resistive losses in the stator winding generates heat and the stator core is equipped with air ducts for cooling. Water cooled generators also exist.

Stator winding

As the alternating flux from the rotor poles passes the coils of the stator a voltage is induced in the coils. The winding is normally a Y connected three phase winding. If a load is connected to the generator this voltage will drive a current through the stator winding and the load.

2.3 Magnetic circuit equivalent

Depending on the aim of the analysis there are several ways of modelling electrical machines and one simple representation is through a magnetic circuit. In article IV this method is used to investigate the effects of an asymmetric field winding.

In figure 2.2 $\mathcal{M}_i$ is the magnetomotive force, MMF, caused by the field winding of each pole. $\mathcal{M}_i$ it is a function of the number of turns of the field

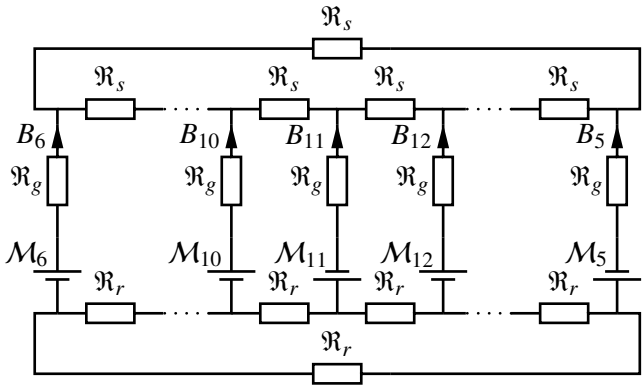

Figure 2.2. Magnetic circuit model of the experiment generator. The MMF for pole eleven, $\mathcal{M}_{11}$, is in article IV given a lower value compared to the other poles.

winding the pole and the field current. $\Re_r$, $\Re_g$ and $\Re_s$ are the reluctances of the rotor, air gap and stator respectively. Reluctance is the magnetic resistance, or equivalently, the inverse of the permeance. B_i is the flux density in the air gap.

3. Eccentricity

Articles II and III investigate different aspects of rotor eccentricity and generator performance. Rotor eccentricity gives rise to unbalanced magnetic pull which puts unwanted stress on rotor and stator supports. It can also cause excessive wear on the rotor bearings. Below follows, as a background to the discussion about UMP in articles II and III , a description of the geometry of rotor eccentricity.

Ideally in a generator the rotor and the stator are perfectly concentric but wear and manufacturing tolerances will inevitably lead to some degree of rotor eccentricity. Other forms of air gap asymmetries, such as non-parallel stator and rotor axes or a non-circular stator, can also occur but this study is limited to rotor eccentricity.

An example of rotor eccentricity is shown in figure 3.1, where the variables used in this chapter also are defined. Rotor eccentricity arises when the stator and rotor centres, O_s and O_r in figure 3.1, do not coincide.

If the displacement d and the direction of displacement α are constant, and not a function of time, the eccentricity is said to be static and the air gap length is a function of the angular position round the air gap only, $\delta = f(\theta)$. In a dynamic eccentricity the centre of the rotor is not fixed and the air gap length is a function of both position and time $\delta = f(\theta, t)$. The investigations in articles II and III and the discussion below are limited to static eccentricity. The air gap length, $\delta(\theta)$, as defined in figure 3.1 is, at any position θ, for a given fixed α

$$\delta(\theta) = R_s - (L_1(\theta, \alpha) + L_2(\theta, \alpha)) \tag{3.1}$$

where R_s is the stator radius and the other symbols are defined in figure 3.1. L_1 can be written as

$$L_1 = d\cos(\theta - \alpha). \tag{3.2}$$

and the distance L_2 is equal to

$$L_2 = \sqrt{R_r^2 - L_3^2} = \sqrt{R_r^2 - (d\sin(\theta - \alpha))^2}. \tag{3.3}$$

where R_r is the rotor radius. Normally d will be small relative to R_r and L_2 will be close to R_r. If R_r is substituted for L_2 the air gap can be written as

$$\delta(\theta) = R_s - (L_1(\theta, \alpha) + R_r) \tag{3.4}$$

which can be rewritten as

$$\delta(\theta) = \delta_0(1 - \epsilon\cos(\theta - \alpha)) \tag{3.5}$$

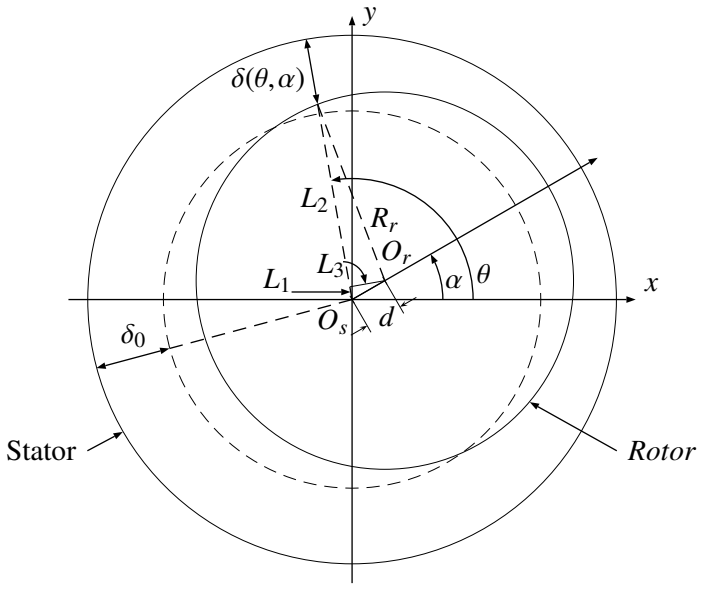

Figure 3.1. An example of a non-centred rotor. O_s and O_r are the axial centres of the stator and rotor respectively. The dashed circle shows the position of a centered rotor. δ_0 is the nominal air gap. The displacement of the rotor relative to the stator is d and the direction of the displacement is α.

where δ_0 is the nominal air gap length and ϵ is the relative eccentricity defined as the displacement divided by the nominal air gap,

$$\epsilon = \frac{d}{\delta_0}. \tag{3.6}$$

3.1 Permeance

The ability of the air gap to conduct magnetic flux, its permeance, is

$$\Lambda_\delta(\theta-\alpha) = \frac{\mu_0}{\delta(\theta-\alpha)}. \tag{3.7}$$

where μ_0 is the permeability of empty space and air is assumed to have a relative permeability, μ_r, of one. If $\delta(\theta)$ is substituted with equation (3.5) Λ_δ can be written as

$$\Lambda_\delta(\theta-\alpha) = \frac{\mu_0}{\delta_0}\frac{1}{1-\epsilon\cos(\theta-\alpha)}. \tag{3.8}$$

The reluctance of the rotor and stator will cause the total permeance of the generator, Λ, to be lower than Λ_δ. At saturated levels of flux density the rotor and stator components of Λ will also be a function of θ. The magnitude of the

permeance and its variation round the air gap causes the unbalanced magnetic pull discussed in articles II and III and it is the rate of change in flux density, which can be modelled by the change in permeance, that drives the damper winding currents in article III.

3.2 Unbalanced magnetic pull

The air gap flux density, B, is a function of the MMF caused by the field winding, M_f, and the total permeance of the generator Λ. M_f is a function of rotor position, i.e. time. However, in a multipole machine it is the length of the air gap that to a large extent will determine the size and direction of the UMP caused by a certain displacement and M_f will hence be treated as a constant below.

In a machine with static eccentricity the direction of displacement, α, is constant and below it has for simplicity been assumed to be zero. The normal, i.e. radial, and tangential magnetic stresses in the air gap are

$$\sigma_n = \frac{B_n^2(\theta) - B_t^2(\theta)}{2\mu_0} \quad \text{and} \quad \sigma_t = \frac{B_n(\theta)B_t(\theta)}{\mu_0} \tag{3.9}$$

where n and t indicates normal and tangential components. At no load it is the normal component which is of interest and with the assumption that B_t is small relative to B_n equation (3.9a) becomes

$$\sigma_n = \frac{B_n^2(\theta)}{2\mu_0} \tag{3.10}$$

If it is further assumed that the permeability of the steel is infinite and hence the permeance of the generator is equal to the air gap permeance the expression for B_n in the equation above can be written

$$B_n(\theta) = \Lambda_\delta(\theta)M_f = \frac{\mu_0}{\delta_0}\frac{M_f}{1-\epsilon\cos(\theta)}. \tag{3.11}$$

Insertion of this expression for B_n into equation (3.10) results in

$$\sigma = \frac{\Lambda^2 M_f^2}{2\mu_0} = \frac{\mu_0 M_f^2}{2\delta_0^2}\frac{1}{(1-\epsilon\cos(\theta))^2} \tag{3.12}$$

where the index n has been omitted.

From the stress the force components in the x and y directions can be calculated as

$$F_x = \int_0^{2\pi} \sigma RL\cos\theta \,\mathrm{d}\theta \tag{3.13}$$

and

$$F_y = \int_0^{2\pi} \sigma RL \sin\theta \, \mathrm{d}\theta \tag{3.14}$$

where R is the average radius of the air gap and L is the length of the generator.

Depending on whether the function for M_f and the relative eccentricity is known or the air gap flux density is known from measurements the total unbalanced magnetic pull for a generator can be calculated from these equations.

4. Finite element analysis

Articles II , III and IV investigated the unbalanced magnetic pull caused by rotor eccentricity and field winding short circuits. The effect of different machine configurations on the UMP was also studied. Parallel to the measurements magnetic field simulations of the experimental generator and generators used in hydropower production were performed using the finite element method.

Four types of materials are used in the simulations: electrical steel, copper, insulation and air. The steel has a variable relative permeability to allow for magnetic saturation. It is also possible to assign different steel qualities to for example the rotor and the stator.

4.1 The field-circuit problem

In the simulations the coupled problems of the magnetic field and the rotor, stator and damper winding electrical circuits are solved simultaneously [4, 5].

Finite element problem

The finite element problem for a generator is set up to solve Ampère's law for the magnetic vector potential, $\mathbf{A}$, in the domain enclosed by the boundary conditions, given the applied field winding current. Because the problem can be represented by a 2D problem $\mathbf{A}$ only has one component, A_z, perpendicular to the xy plane.

Between the nodes of the elements in the mesh the solution is found through interpolation of the base functions. These functions can be linear quadratic or of higher order. The work presented here mostly employs linear base functions but quadratic functions have been used for comparisons.

Circuit equations

The magnetic flux from the solution of the finite element problem induces a voltage in the damper and stator windings of the generator. Through the circuit equations for the stator and damper windings the resulting currents in the windings are calculated. These currents affect the flux density and in the coupled problem the circuit equations are solved together with the finite element problem in an iterative process. When a solution is found for a time step the solver proceeds to the next time step.

4.2 Geometry

2D finite element analysis was used in the articles mentioned above. Two benefits of 2D simulations compared to 3D simulations is the reduction in computational time and the relative ease with which the geometry can be implemented.

In simulations of a machine with a symmetric air gap flux density the geometry can often be reduced to one or two poles, equivalent to a half or a full electrical cycle. Fractional slot windings might require a larger part of the machine to be modelled. When a non-uniform air gap or a machine with an otherwise asymmetric air gap flux density is studied simulation of the full geometry is required.

Mesh and boundary conditions

The principle of the finite element method is to divide the analysed area into a large number of small elements and to find a solution for the field equation for each element. All elements taken together form the mesh. Figure 4.1 contains a section of the generator geometry and the mesh. To avoid remeshing at every time step during dynamic simulations the rotor and stator are meshed individually and a sliding mesh interface is used between them. A uniform mesh element size is used in the air gap to allow for the sliding mesh. In figure 4.1 it can also be seen that the mesh element sizes vary and are smaller where the geometry contains complex detail.

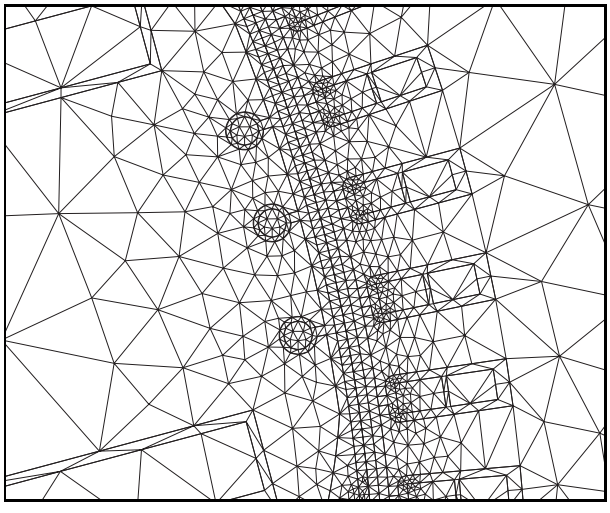

Figure 4.1. A section of the air gap. One of the poles with its three damper bars can be seen to the left in the pictures. The stator with its coils make up the right half of the picture. The elements on each side of the middle of the air gap have equal tangential length to allow for the sliding mesh.

The boundaries of the finite element problem are shown in figure 4.2. The area studied is limited by the inside of the rotor ring as the inner boundary and the stator back as the outer boundary. Outside this domain the material, air, has a low permeability relative to the steel in the generator and the flux density is assumed to be zero. The effect of this is that no flux can escape the area enclosed by the boundary conditions or, equivalently, at the boundary the homogeneous Dirichlet condition $A_z = 0$ states that the field lines has to be parallel to the boundary.

The interface of the sliding meshes of the rotor and the stator are shown by the blue line in figure 4.2.

When a section of the generator is simulated it is common to put periodic boundary conditions on the section boundaries that are parallel to a radius taken from the machine centre. Periodic boundary conditions are not used in the simulations of a full machine geometry presented here.

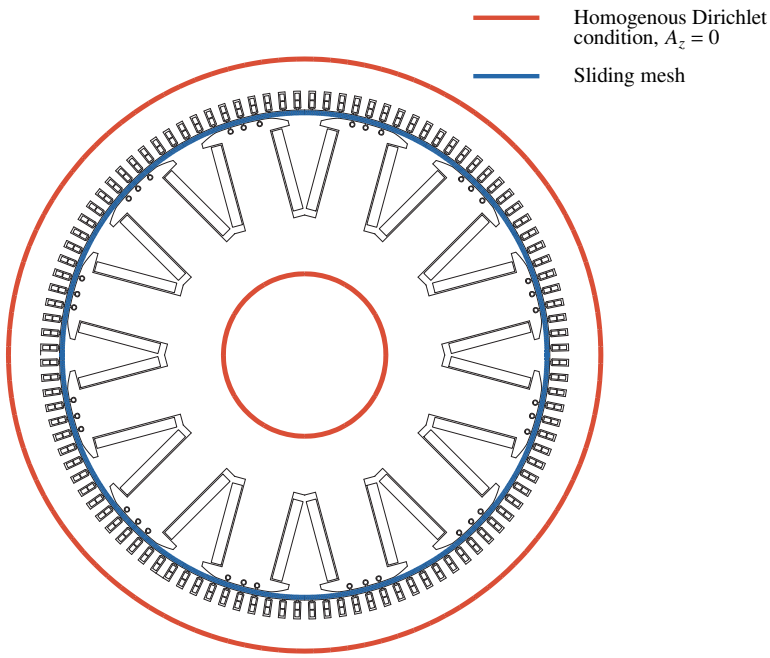

Figure 4.2. The boundaries of the finite element solution. The red circles represent homogeneous Dirichlet conditions, $A_z = 0$, while the blue line indicates the sliding boundary between the rotor and the stator meshes.

Three-dimensional effects

Phenomena which are overlooked in 2D analysis are for example three dimensional effects such as eddy currents in the rotor and stator steel, nonlinearities

in the magnetic flux and the flux leakage impedance caused by air ducts [6] and end effects, e.g. end flux leakage and coil end inductances. End effects increase in importance when the machine has a large diameter relative to its length. Hydropower generators commonly have a high diameter to length ratio compared to turbo generators and end effects should not be ignored when studying the former. Coil end inductances can for example be included in the coupled circuit described in section 4.1.

Eccentricity

The eccentricity used in articles II and III was implemented with the variable permeance method described in [7]. Instead of changing the air gap length, δ, in the calculation of the permeance, $\Lambda_\delta = \mu_0\mu_r/\delta$, the relative permeability, μ_r, previously assumed to be one, is changed round the air gap to obtain the equivalent effect on the flux density. With this method it is possible to simulate dynamic eccentricities at other frequencies than the synchronous as well as irregular air gaps without remeshing the geometry at every time step.

4.3 Solutions

After the solution for A_z has converged, either in a static or a dynamic simulation, post-processing is used to extract more information from the solution. The magnetic pull and the torque are calculated through the Maxwell stress tensor from the normal and tangential flux densities in the air gap. For the tangential flux density an average is taken over part of the air gap in a method similar to the one proposed in [8]. The voltages and currents in the generator windings are also calculated.

5. Research areas

5.1 Parallel circuits and rotor eccentricity

Multipole synchronous generators are often equipped with parallel circuits in the stator winding to reduce current density and resistive losses. In article II the effect of parallel stator circuits on the UMP caused by rotor eccentricity is studied. The experiment required the stator winding to be divided into two separate circuits. In this study both FE simulations and an analytical model based on a varying permeance in the air gap were used together with the measurements. A relative eccentricity of 24 percent was used in both measurements and simulations.

Configurations

Figure 5.1 contains an overview of the two stator winding configurations used in the experimental generator. The division is placed parallel to the x axis. Hydropower generators will often have more than two circuits and each circuit can be distributed over more than one section of the stator. Phase a will be used in the discussion below but phases b and c are treated analogously. When the two circuits are connected in series, per phase, the result is a single circuit stator winding as shown in figures 5.1(a) and 5.2(a).

With points a_1 and a_2 unconnected the generator has two separate circuits and it is possible to measure the two circuit voltages separately. In the configurations with two circuits on the experimental generator the terminal voltage will, for any given field current, be half of that of the single circuit configuration. When the circuits are connected in parallel the total current drawn by a load can be twice as high without an increase of the current density, and resistive losses, in the stator coils. The measurements and simulations were performed with a relative eccentricity of 0.24, a field current of 15 A and without the damper winding mounted.

Parallel circuit voltage

As shown in chapter 3 the non-uniform permeance caused by the rotor eccentricity will result in a varying flux density round the circumference of the generator. This variation in flux density can, if the stator winding consists of two or more parallel circuits, induce different voltages in the stator circuits.

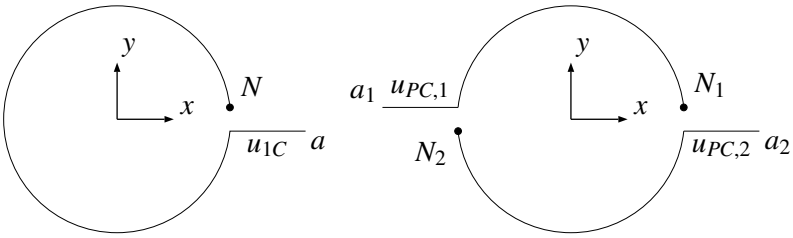

Figure 5.1. With each phase winding divided into two sections it is possible to connect the sections either in series or in parallel. *N* stands for neutral. Phases *b* and *c* are not depicted in the graph.

The stator voltage is induced by the varying flux in the air gap and it is therefore, at a given rotational speed, proportional to the flux density shown in equation (3.11). Displacement of the rotor in the direction y, $\alpha = 90°$ in figure 3.1, will result in the largest flux density difference, and generate the largest voltage difference, between the two circuits. A first order Taylor approximation and integration of equation (3.11) shows the effect of the eccentricity on the parallel circuit voltage

$$u \propto K \int_a^b \frac{1}{1 - \epsilon \cos(\theta \alpha)} \, \mathrm{d}\theta \approx K \int_a^b 1 + \epsilon \cos(\theta - \alpha) \, \mathrm{d}\theta \tag{5.1}$$

where K is a proportionality constant. If the integral is taken for the two halves of figure 5.1(*b*), i.e. from 0 to 180 degrees, and from 180 to 360 degrees the results are

$$u_{PC,1} \propto K \int_0^{\pi} 1 + \epsilon \cos(\theta - \pi/2) \, \mathrm{d}\theta = K(\pi + 2\epsilon) \tag{5.2}$$

and

$$u_{PC,2} \propto K \int_{\pi}^{2\pi} 1 + \epsilon \cos(\theta - \pi/2) \, \mathrm{d}\theta = K(\pi - 2\epsilon) \tag{5.3}$$

where the integration intervals are given in radians instead of degrees. From equations (5.2) and (5.3) it can be seen that when the rotor is displaced in the y direction the voltage difference between the two circuits is proportional to the degree of displacement, ϵ.

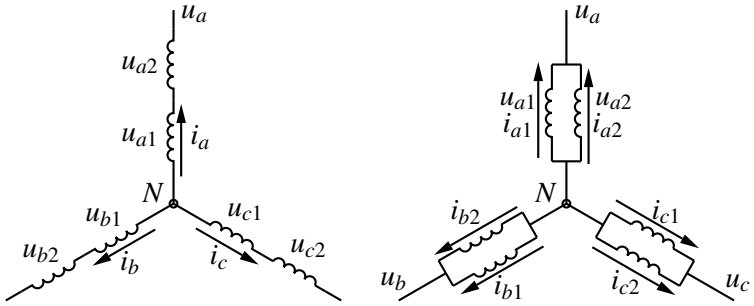

Figure 5.2. The two possible stator configurations. In the configuration to the right, i_{a1} and i_{a2} must be equal during no-load operation.

Parallel circuit currents

Parallel connections between the phases of the two circuits, shown in figure 5.2(*b*), will force the voltages to be the same in the two circuits. It will also allow for intrastator currents driven by the induced voltage difference to flow between the circuits. These currents do not contribute to the power delivered by the generator but they do contribute to the resistive losses.

Another consequence of the parallel circuit currents is a reduction of the difference in flux density between the two halves of the air gap and hence a lowered UMP in equations (3.13) and (3.14).

5.2 Damper windings and rotor eccentricity

Damper windings can reduce the UMP caused by rotor eccentricity [9] and damper winding influence on UMP is discussed in article III. The measurements and simulations were performed with a relative eccentricity of 0.44, a field current of 15 A and without the damper winding mounted.

Configurations

A production generator will typically have five to seven damper bars. Two forms of damper winding connections are common. In the first configuration only the damper bars within a pole are connected, through a short circuiting connector or plate, and the only path for any interpole damper currents are through the contact between the damper bars and the iron components of the rotor. This configuration is called a partial or a grill damper winding. The other alternative is a complete damper winding where the damper bars of each pole are directly connected to the bars of the adjacent poles at both ends of the machine through end ring segments. In the literature the expression amortisseur winding is often used instead of damper winding.

Four damper winding configurations were used in the measurements on the experimental generator. Including the reference measurement of the UMP at standstill the configurations were:

1) standstill.
2) without damper winding (WD).
3) with a continuous damper winding with damper bar 2 only (D2-C).
4) with a non-continuous damper winding with damper bars 1 and 3 (D13-NC).
5) with a continuous damper winding with damper bars 1 and 3 (D13-C).

Short theory

When a machine equipped with a partial damper winding is subject to static rotor eccentricity the varying flux density in the air gap induces a voltage in the damper bars. The resulting current creates an MMF which strives to counteract the change in flux density; when the flux density is increasing the flux caused by the damper MMF is opposing the air gap flux, and conversely, when the air gap flux density is decreasing the damper winding induced flux is added to the air gap flux.

The magnitude of the induced damper winding voltage, U_{D} is a function of the rate of change of the air gap flux density and therefore proportional to the derivative of the air gap permeance described by equation (3.8). With α set to zero in (3.8) the relationship is

$$U_{\mathrm{D}} = A \frac{M_f \mu_0}{\delta_0} \frac{-\epsilon \sin(\theta)}{(1 - \epsilon \cos(\theta))^2} \tag{5.4}$$

where A is the damper winding area and it has been assumed that the flux density is uniform over the width of the damper winding. In section 7.5 the measured damper winding voltage is fitted to this equation.

Damper winding currents

The equations above are correct for an idealised situation with a partial damper winding and does not account for stator slot ripples or the effect of eddy currents on the air gap flux density. To obtain more information about the effect of damper windings on UMP and the magnitude of the currents in the damper winding both simulations and measurements of different damper winding configurations were performed.

On the experimental generator it is possible to choose between one, two and three damper bars and to select whether or not to connect the damper bars on adjacent poles. The damper bar positions in the pole shoe on the experimental generator can be seen in figure 5.3.

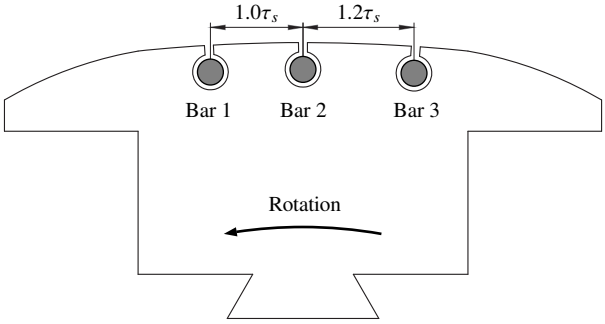

Figure 5.3. The position of the damper bars seen from above.

5.3 Field winding interturn short circuit

In article IV the UMP was caused not by rotor eccentricity but by a short circuit between one or more field winding turns on one of the poles. Ageing and mechanical wear of the field winding insulation can result in electrical contact between field winding turns. The result is a rotating unbalance which can excite vibrations in the generator.

Configurations

Various degrees of field winding interturn short circuits were measured. The flux Φ in a magnetic circuit is

$$\Phi = \frac{NI}{\Re} \tag{5.5}$$

where N is the number of turns in the coil, I the current in the coil and $\Re$ is the reluctance of the magnetic circuit.

In the FEM simulations the reduction in Φ was accomplished through a reduction of N in the field winding for one pole, while on the experimental generator, some of current, I, was shunted past one pole through a resistor parallel with the pole field winding. The configurations are REF, 4.3, 9.5, 17 and 30 where REF is the unmodified rotor and the numbers refer to the reduction in ampere turns in percent on pole eleven.

Unbalanced magnetic pull from field winding short circuit

The effect on the air gap flux is described in chapter 7 and in article IV. A UMP which rotates with the mechanical frequency caused by the reduced flux from the affected pole is detected. Another observation is that the unaffected poles with the same polarity as the damaged pole experience an increase in flux density. The effect is seen in the measurements, the finite element calculations and in the simple magnetic circuit representation of the generator depicted in figure 2.2.

5.4 Standstill frequency response test

In article V a standstill frequency response, SSFR, test on the experimental generator is performed to identify the machine transfer functions. Unlike the standard SSFR test, which is described in [10], the study presented in article V includes measurements of damper winding currents and voltages. This required a redefinition of the damper equivalent circuit from the form representing the physical damper winding to a dq representation. The new equivalent winding is described in section II of article V.

Configurations

In the test a voltage with varying frequency is applied to two of the stator phases while the third is left open. The result is a magnetic flux in the air gap which fluctuates in amplitude but does not rotate. The test is performed with the rotor in the direct, d, and the quadrature, q, axis positions.

The test was performed with the applied voltage varying in frequency from 5 mHz to 300 Hz. Complete and partial damper winding configurations were used as well as a rotor without any damper winding.

It is stressed in [10] that the stator winding must keep a constant temperature so the test is performed at current levels which are only a fraction of the rated levels. Hence the obtained parameters do not include effects of magnetic saturation.

6. Experimental generator

All articles included in this thesis contain measurements from the experimental generator Svante at the Division of electricity at Uppsala university. The construction of the generator represent a substantial part of the work behind this dissertation. Article I describes the construction of the generator. This chapter contains some additional information and includes work done after the publication of the article.

6.1 Construction

The construction process started with the donation of a twelve pole three phase vertical axis synchronous motor to the division.

Original motor

Other characteristics of the machine was that it had salient poles with solid pole shoes and that the rating was 185 kW at 380 V and a $\cos\varphi$ of 0.9. As an experimental machine the motor was not very suitable in its original configuration since very few components were accessible for measurements and there were no adjustment capabilities to modify parameters of interest. On the other hand, the machine was in good condition and perfect as a base for a test setup.

A few modifications were made to the rotor and the stator of the motor to turn it into a generator more similar to hydropower production machines and to allow for the reconfigurations needed for various experiments. The rotor and the stator were also individually suspended to allow for measurement of the magnetic pull in the air gap.

Rotor

To reduce the risk of the rotor coming into contact with the stator during non-centered operation the average air gap was increased through a reduction of the pole body height. Given that there had to be room also during non-centered operation for the air gap flux density sensors a longer air gap allowed for a larger relative eccentricity. It was also easier to implement certain relative eccentricity on a larger air gap. Finally, a larger relative eccentricity increased the signal to noise ratio in some of the experiments that were planned.

Laminated pole shoes

Laminated poles and rotor rings are standard on large hydropower generators [11]. On the experimental generator the original cast rotor was kept but, as the pole bodies were shortened more than was required for the increased air gap length, laminated pole shoes could be mounted. The laminated pole shoes serve to reduce the eddy currents in the pole face resulting from variations in the air gap flux density. Under most circumstances the rotor poles are subject to a smaller variation in the flux density than the stator, which sees a complete reversal of the magnetic field every electric cycle, and therefore the lamination thickness is often thicker in the rotor than in the stator. The pole shoes of the experimental generator were made of 2 mm varnished sheet steel compared to the 0.5 mm original steel of the stator. Figure 6.1 shows the shape of the laminated pole shoe and figure 4 in article I shows the geometry of the pole shoe mounted on the pole body.

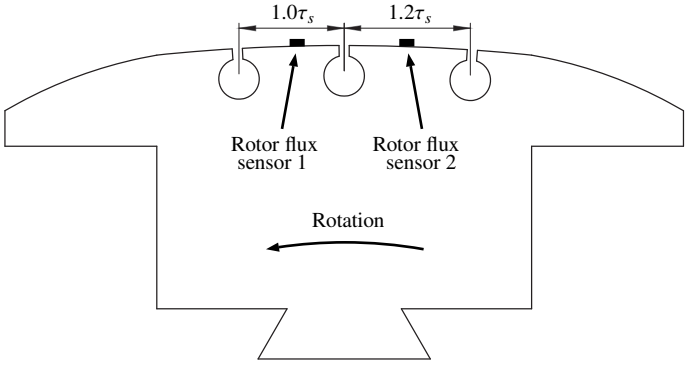

Figure 6.1. Two air gap flux sensors was mounted on one of the poles. The signals was transmitted to a stationary computer through the wireless module shown in figure 6.9.

Damper winding

One of the main experiments the generator was built for was to investigate the effect of a damper winding on the reduction UMP. The rotor was therefore equipped with a removable and reconfigurable damper winding. A cross section of a pole body with the pole shoe and the damper bar slots is shown in figure 6.1. The damper bar slots were not distanced evenly but rather with the separation of 1 and 1.2 stator slot pitches. This was done so that the effect of damper bar pitch on stator voltage total harmonic distortion, THD, could be investigated.

An example of a damper winding configuration is shown in figure 6.2. Here two damper bars, out of three possible, and the inter-pole connectors are used. The damper bars and the inter-pole connectors are all attached to a copper bar at each end of the pole. The damper bars are insulated from the pole plates by

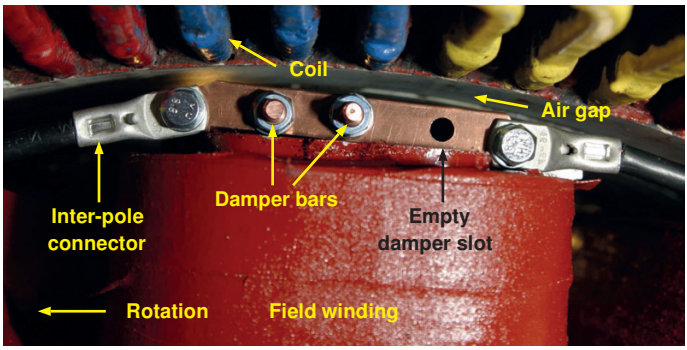

Figure 6.2. Inter pole connectors as well as individual damper rods can be removed. In the figure two out of three possible damper bars are mounted leaving one position empty.

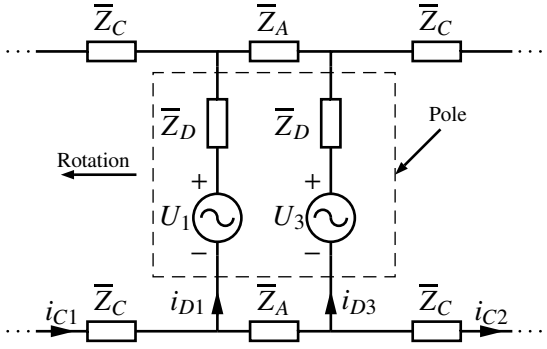

Figure 6.3. Circuit diagram of a section of a complete damper winding with two damper bars per pole seen from the rotor shaft. The interpole connectors are represented by the impedances $\overline{Z}_C$. The direction of rotation is anticlockwise

heat shrinkable sleeves. Figure 6.3 contains the circuit diagram for a complete damper winding with two damper bars.

Stator

The stator could be used as it was with the exception of a division of the double layer concentric winding into two circuits to enable the parallel circuit experiment described in article II .

Stator suspension

Adjustable rotor eccentricity and measurement of UMP required independent suspension of the rotor and the stator. Either the rotor or the stator had to be suspended in a way that allowed measurement of the radial forces. A motor and gear box had to be connected to the rotor so it would have been difficult to suspend that part of the generator. It was decided that the vertical axis con-

figuration of the machine would be kept and that stator should be suspended in steel rods with ball joints at the ends.

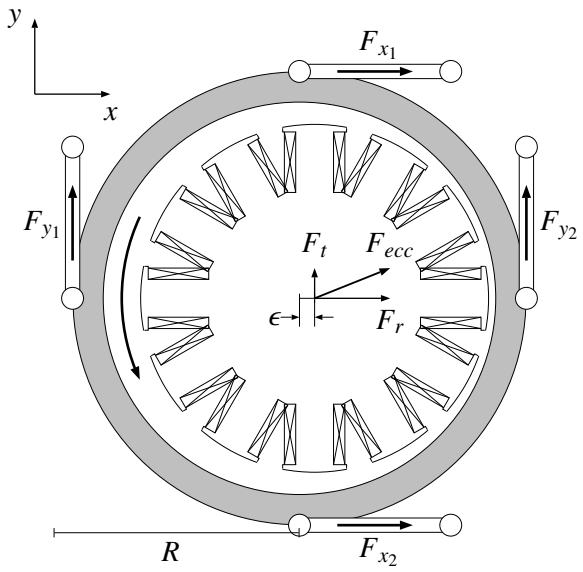

Figure 6.4. The radial support of the stator seen from above.

One benefit of this solution was that keeping the axis vertical made it possible to reuse the old bearings, which were in good condition. Other items that were used directly from the motor were the slip rings and the brushes. A new attachment for the brushes' spring mechanism was however built. New housings for the bearings also had to be made.

The geometry of the stator suspension is shown in figure 6.4. From the measured forces it is also possible to calculate the mechanical torque on the generator.

Parallel circuits

The physical separation of the stator winding into two halves was performed by cutting the connectors between the coils instead of cutting the coils themselves. With this solution the connectors required to alternate between one- and two-circuit operation was greatly reduced. The two possible stator winding configurations are shown in figure 5.2.

Svante

Figure 6.5 shows a drawing of the resulting machine with a few of the components labelled. Worth noting is that the rotor is fixed and that the stator is suspended in such a way that it can be moved horizontally. All components seen in figure 6.5, except for the motor and gearbox, were designed from the

geometry of the donated motor and the desired capabilities of the experimental generator. Some of the data for the resulting machine are listed in table 6.1.

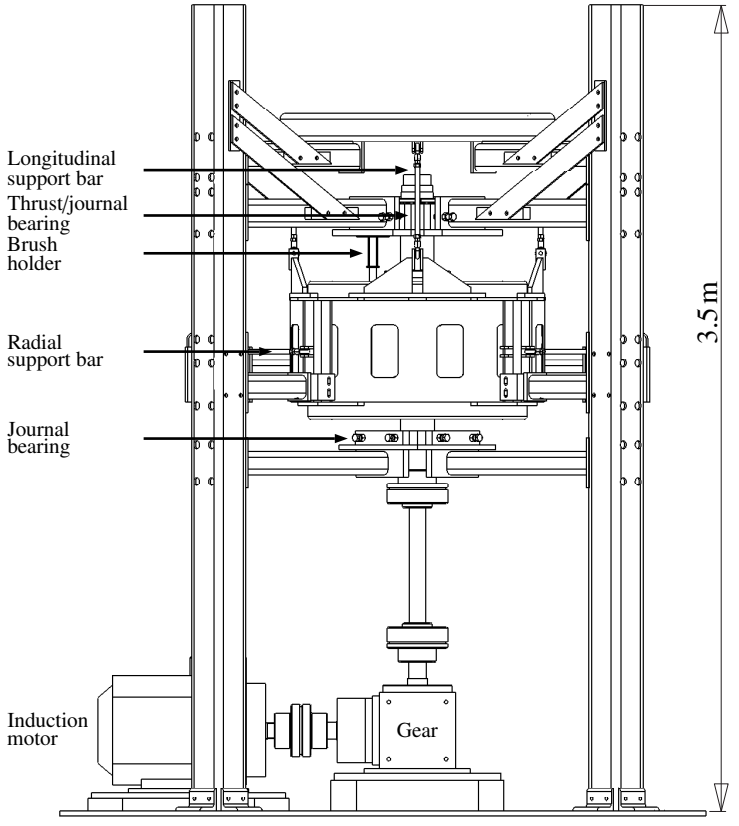

Figure 6.5. A structure was built to independently suspend the rotor and the stator. The figure shows how the rotor rests on a thrust bearing and stator is suspended in metal bars. One horizontal beam in front of the stator has been removed from the drawing for clarity.

Drive, motor and gear box

A 75 kW induction motor and an inverter were used to power the generator. The motor had four poles whereas the generator had twelve and a 3:1 gearbox was installed between the motor and the stator to give a suitable working speed for the induction motor and its inverter during synchronous operation of the generator.

Magnetisation equipment

The field current can be supplied either a by purpose built rectifier or from a controlled laboratory supply. The former was used in articles I and II .

Table 6.1. *Main parameters for the refitted test generator.*

Frequency	50 Hz
Number of pole pairs	6
Speed	500 rpm
Slots per pole and phase	3
Number of stator slots	108
Coil pitch	9
Stator inner diameter	725 mm
Stator length	303 mm
Air gap length	8.4 mm
Power of driving motor	75 kW
Rotor weight	900 kg
Stator weight	700 kg

Synchronisation equipment

Synchronised operation is the usual mode of operation for hydropower generators and synchronisation equipment has been installed on the test setup to create realistic load conditions. Grid connected operation also enables research into generator-grid interaction.

A resistive load has also been installed to free the generator from constraints on for example voltage and rotational velocity during operation under load. The symbols in figure 6.6 are explained in table 6.2

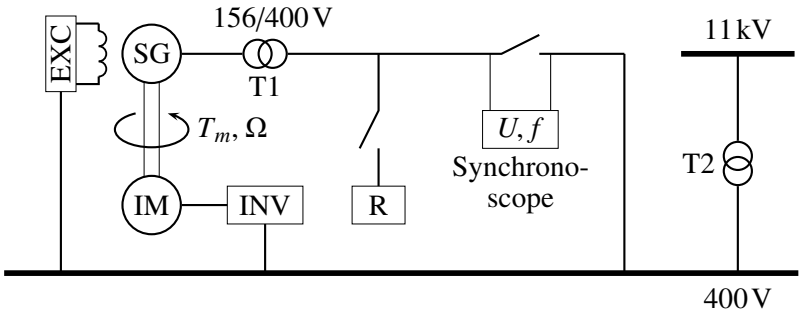

Figure 6.6. A schematic of the experimental generator, its drive and the connection to the grid. The symbols are explained in table 6.2.

Table 6.2. *Symbols used in figure 6.6.*

EXC	Field winding exciter
f	Grid and generator frequency comparison
IM	Induction motor
INV	Inverter
R	Resistive load
SG	Synchronous generator
T1	156 V to 400 V transformer
T2	400 V to 11 kV transformer
T_m	Mechanical torque
U	Grid and generator voltage comparison
Ω	mechanical frequency

6.2 Measurements

The experimental generator was built to study electromagnetic phenomena as well as to validate the finite element software described in chapter 4. To achieve this several types of sensors were mounted on both the stationary and the rotating parts of the generator.

All measurements presented in articles I–IV were collected as voltage signals and stored at a rate of 10 000 samples per second. In total 28 signals were used. Apart from an amplification of the strain gauge signals no filtering or other form of signal manipulation was performed on these signals.

Measurements were taken with differential channels and sensors were, wherever possible, kept floating. Twisted pair signal cables were used.

In article V additional temporary measurement points were used. In the article the amplification of the signals from the induced damper and field winding voltages and currents and the data collection frequency were selected depending on the frequency of the applied voltage.

Non-rotating measurements

Not all measurements below were available in every experiment, there was for example no damper voltage signal available during damper current measurements, but all available measurements were recorded.

Stator air gap flux

Hall sensors were attached to two stator teeth 90 mechanical degrees apart. The sensors were powered with a constant current of 1 mA. The angular separation of the sensors would cause them detect different levels of flux density during non-centered operation. Hall sensors were selected instead of search coils because of their ability to measure a constant flux level and because of their higher resolution [12].

Stator voltages
The parallel circuit voltages could be measured separately during no load operation with two stator circuits. Each phase was monitored and in total six channels were dedicated for stator voltage measurements.

Stator currents
Three Hall effect current transducers were mounted to measure intrastator currents in each phase during parallel circuit operation. Another three transducers were measuring the current from the generator during operation with load.

Stator forces
Strain gauges were used to measure the forces on the stator. They were positioned so that amplitude and direction of the UMP as well as the torque on the generator could be calculated from the recorded data. Figure 6.4 contains a schematic of the geometry. Four strain gauges were mounted in a full Wheatstone bridge on each of the four rods. The signals for the four bridges were then amplified individually before being stored together with the other measurement data. The linearity of the strain gauges and the gain of the amplifiers have been calibrated with known weights. Figure 6.7 contains a photograph of one of the four rods used to fixate the stator radially. The positions of the rods on the stator can be seen in figure 6.4.

Figure 6.7. The stator was secured radially with four 16 mm metal rods. Figure 6.4 shows the position of the rods. Each rod was equipped with four strain gauges in a wheatstone bridge.

Rotating measurement equipment

Measurements collected on the rotor were transferred via wireless LAN to the measuring computer.

Rotor air gap flux
Two Hall sensors, of the same type as used on the stator, were mounted on one of the poles. At eccentric operation these sensors detect a varying flux density over one mechanical revolution. They also detect the stator slot ripple in the air gap flux density. The position of the rotor flux sensors are shown in figure 6.1.

Damper winding voltage
With the damper winding replaced with open circuit conductors the voltage induced in the damper bars was measured.

Damper winding currents
On one pole current Hall sensors were placed around the damper bars and interpole connectors. There were three sensors for the damper bars and two for the interpole connectors. Figure 6.8 is a photograph of the housing in which the currents sensors were mounted. The positions of the sensors coincide with the current arrows in figure 6.3. $\overline{Z}_C$ in the figure represent the removable interpole connectors.

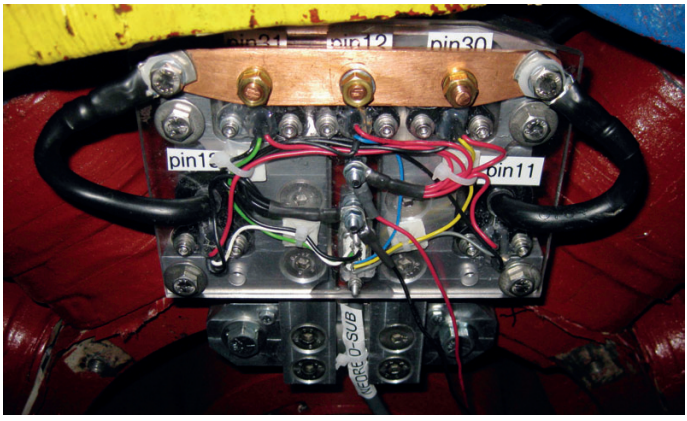

Figure 6.8. On one of the poles the damper bar and connector currents were measured with Hall effect current transducers placed on the lower side of the rotor. A sensor is mounted around each damper bar above the flat copper piece. The interpole connectors, the two black cables, pass through two more current sensors.

Wireless data transfer
The data collected on the rotor was transferred through a WLAN connection to the stationary measurement computer. To minimise the g-forces on the transmitter and have a free line of sight from the aerial to the stationary computer it was mounted directly on the top end of the rotor axle, as shown in figure 6.9.

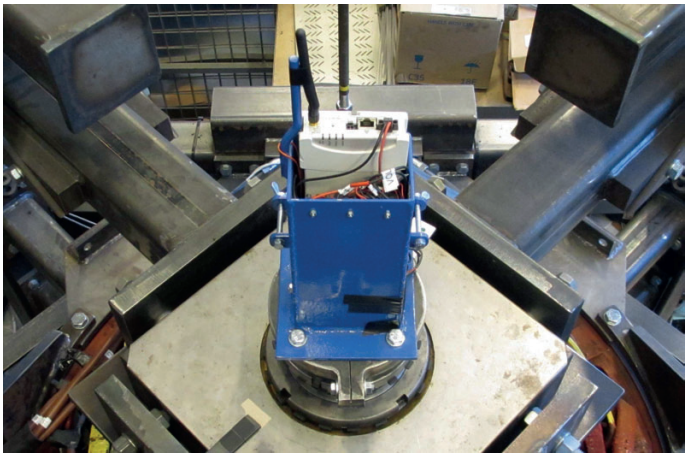

Figure 6.9. Data collected on the rotor was transferred wirelessly to the stationary logging computer. The transmitter was placed on top of the rotor axle.

7. Results

The results from the four research areas presented in chapter 5 can be found in their respective articles II–V. This chapter contains the most interesting findings from articles II–IV and some additional material not included in the articles.

7.1 Magnetic saturation

Hydropower generators are normally operated at some degree of magnetic saturation but to avoid nonlinear effects from saturation on the measurements all experiments were carried out at unsaturated levels of magnetic flux density.

One way of finding the magnetisation where the iron is starting to saturate is to plot the no-load voltage curve and see at which field current the relationship between the terminal voltage and the field current ceases to be linear. Figure 7.1 contains the line to line voltage of the experimental generator as a function of the field current. To within measurement accuracy there was no detectable saturation at field currents below 15 A and all experiments were performed at a field current of 15 A or lower. The correct voltage for synchronisation with the grid, through the transformer shown in figure 6.6 was obtained at a field current of 13 A.

The no-load voltage curve was also used to get the correct shape for the *BH* curve used in the simulations. Due to the unknown materials of the rotor and the stator the terminal voltage and flux density of the simulations did not initially agree with the measurements but from the measured *BH* curve it was possible to obtain simulated values which corresponded well with the measurements.

7.2 Parallel circuits and rotor eccentricity

Section 5.1 described the parallel circuit configuration of the experimental generator. It was also mentioned that in addition to FE simulations an analytical permeance model was used to study the effect of parallel stator circuits. This study was performed before the air gap flux density sensors had been mounted on the experimental generator. The shortest air gap is positioned at 180 degrees in the plots. For a more detailed presentation of the parallel circuit study please see article II.

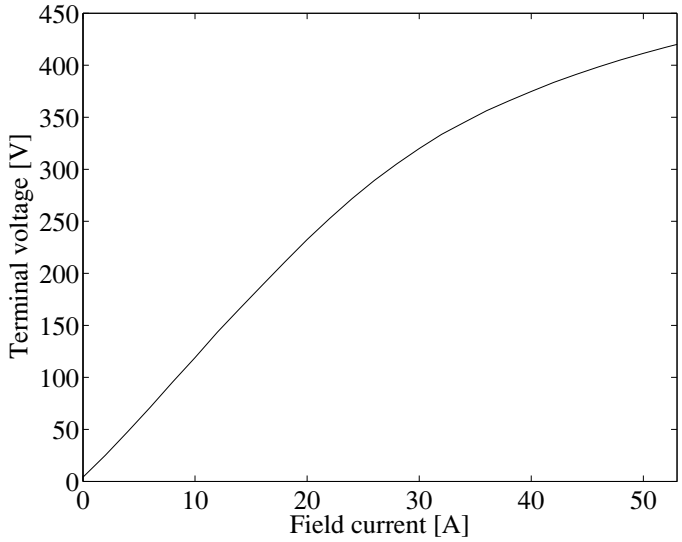

Figure 7.1. The no-load voltage. All experiments were carried out at a field current of 15 A or lower to avoid effects of magnetic saturation.

Effect on unbalanced magnetic pull

With the rotor displaced parallel to the symmetry line of separation of the two circuits, the x axis in figure 5.1, the effects on UMP and terminal voltage were negligible but when the stator was displaced perpendicular to the symmetry line, the y axis in figure 5.1, a large reduction of the UMP could be observed. The results are summarised in table 7.1. The effect of eddy currents are not included in either of the computer models so the UMP at standstill is the same as for the configuration with one circuit.

Table 7.1. *UMP reduction from parallel circuits with the eccentricity perpendicular to the symmetry line.*

Configuration	Measured	FEM	Permeance model
Standstill F_y [N]	4250	-	-
One circuit F_y [N]	3216	4115	4072
Two circuits F_y [N]	1345	1734	1774
Reduction relative to one circuit F_y [%]	58	58	56

Parallel circuit voltages

Figure 7.2 contains the voltages of the two parallel circuits when the rotor is displaced parallel to the y axis. Due to the difference in the average flux density for the two circuits the induced circuit voltages are not equal. In the

figure circuit one, with the on average shorter air gap, is represented by solid lines for phases a, b and c. The average rms voltage difference between the two circuits is 19 percent. The simplified circuit voltages of equations (5.2) and (5.3) predicted a difference of 31 percent. Two explanations of the discrepancy are the linearisation of the equations and an error in the measurement of the relative eccentricity used in the equations.

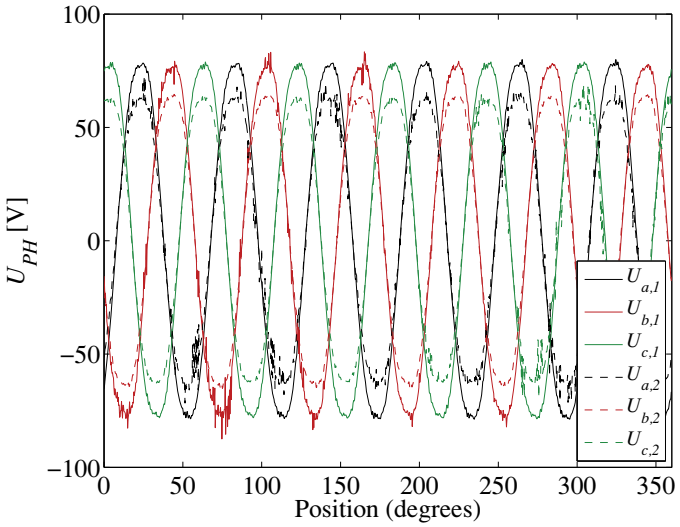

Figure 7.2. The open circuit voltages measured at a relative eccentricity of 0.24 and a field current of 15A for the two stator circuits. Circuit one, represented by the solid lines, had an, on average, smaller air gap and hence larger total flux than circuit two. The result is a difference in the induced voltages in the two circuits. The layout of the circuits are shown in figure 5.1.

Parallel circuit currents

The induced voltage difference between the two halves of the stator winding will, if the two winding sections are connected in parallel, drive intrastator currents. The measured currents from such an experiment are shown in figure 7.3. An effect of these currents is a reduction in the air gap flux density difference between the two halves of the stator. It is this reduction in flux density difference which causes the reduction of the UMP shown in table 7.1.

During the experiment the generator was operated at no-load and, besides reducing the UMP, these currents only result in resistive losses.

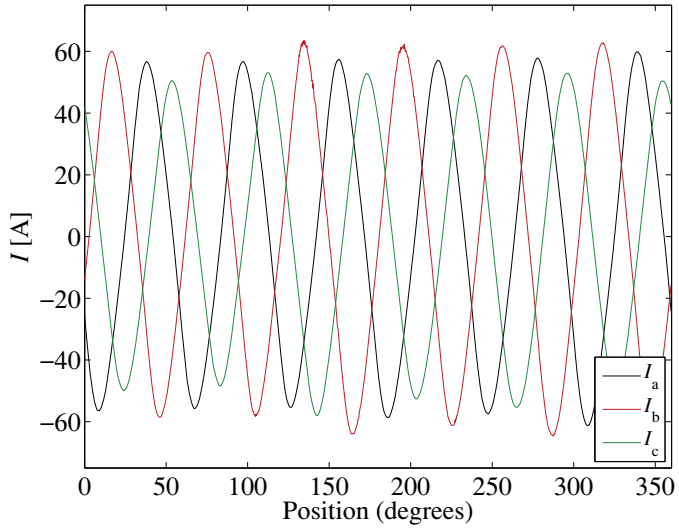

Figure 7.3. The parallel circuit currents driven by the difference in induced voltage between the two stator halves shown in figure 7.2. Measurements were taken at no-load.

7.3 Damper windings and rotor eccentricity

Article III describes the effect of different damper winding configurations on UMP during rotor eccentricity. A description of the damper winding configurations and the terminology used here can be found in section 5.2. Below follows a brief summary of the findings from the article. The shortest air gap is positioned at 180 degrees in the plots.

Effect on unbalanced magnetic pull

The resistance of the damper windings and the fraction of the pole face area covered by the damper winding were, through simulations, found to have a large influence on the reduction of the UMP from the damper winding. With the damper winding currents from the experimental generator the effect on the UMP was negligible. All experiments and simulations were carried out at field current of 15 A and a relative eccentricity of 0.44.

Table 7.2 contains the simulated forces resulting from the four configurations described in section 5.2. In these simulations of the experimental generator the damper winding resistances were set to result in the same damper winding currents as in the measurements.

As a comparison a 28 pole generator used in hydropower production, with a damper winding covering a large fraction of the pole face, was studied in simulations. The damper winding resistances were set to values calculated from material resistivity only and no contact resistances were included, much

as would be the case for a generator with a soldered damper winding. The resulting large reduction in UMP can be seen in table 7.3. In the table it is also possible to see that a relatively large tangential force component, approximately a quarter of the total remaining UMP, is introduced by the damper winding. In neither the experimental nor the production generator does the presence of damper winding interpole connectors have a large influence on the UMP. The level of interpole connector currents in the experimental generator can be found in article III. In the production generator they were approximately an order of magnitude less than the damper bar currents.

Table 7.2. *Simulated UMP change on the experimental generator for the studied damper winding configurations. The last column is the change in UMP compared to the configuration WD. The notation WD, NC and C are described in section 5.2.*

Configuration	F_x [N]	F_y [N]	F_{ecc} [N]	ΔF_{ecc} [%]
WD	9174	-1	9174	-
D2-C	9192	35	9192	0.2
D13-NC	9156	139	9157	-0.2
D13C	9150	188	9152	-0.2

Table 7.3. *Simulated UMP change on a 28 pole production generator for the studied damper winding configurations. The last column is the change in UMP compared to the configuration WD. D1-7 indicates that all seven damper bars per pole were used.*

Configuration	F_x [N]	F_y [N]	F_{ecc} [N]	ΔF_{ecc} [%]
WD	325800	300	325800	-
D1-7-NC	184600	49250	190670	-41.5
D1-7-C	184200	49000	190220	-41.6

7.4 Field winding interturn short circuit

Unbalanced magnetic pull caused by field winding interturn short circuit, described in section 5.3 was studied in article IV. The experiments were performed with a centered rotor at a field current of 15 A. In the figures the index REF indicates the magnetically symmetric rotor and the numbers the degree of interturn short circuit on pole eleven.

Resulting unbalanced magnetic pull

A winding interturn short circuit on one of the poles results in a reduced flux density for the pole. Figure 7.4 contains the absolute air gap flux densities

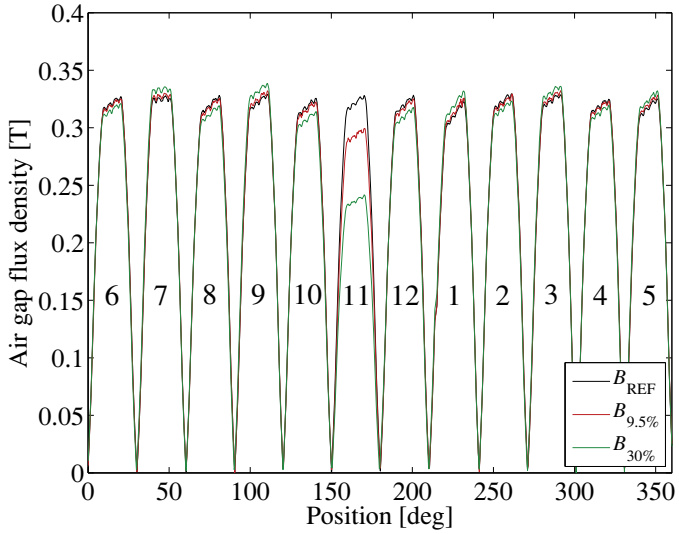

Figure 7.4. The absolute air gap flux density from the magnetically symmetric rotor and two of the interturn short circuit configurations.

for the unmodified rotor and for two of the reductions in ampere turns on pole eleven, as measured on a stator tooth. In this figure an interesting feature is the effect the damaged pole has on the flux density of the other poles. The reduction of ampere turns on pole eleven reduces the total number of ampere turns on the rotor and hence the total flux in the air gap. Gauss's law for magnetism states that the magnetic field is divergence free and hence the conservation of flux has to hold. In this situation the total flux for the odd numbered poles, with the same polarity as the affected pole, and the even numbered poles, having the opposite polarity, must be equal. All even numbered poles in figure 7.4 exhibit a lowered flux density as expected from the reduction in the total number of ampere turns. At the same time the odd numbered poles, except for pole eleven, experience an increase in flux density to compensate for some of the reduction in the flux density of pole eleven.

One result of the asymmetric flux is a pull on the rotor in the opposite direction of the affected pole. Table 7.4 contains, among other quantities, the measured and simulated unbalance forces caused by different levels of field winding interturn short circuit on one of the twelve poles on the experimental generator. The corresponding measured force orbits can be seen in figure 7.5.

Flux from a magnetic circuit model

A magnetic circuit calculation, derived from the circuit in fig 2.2, of the effect of interturn field winding short circuit on pole flux was also performed. To simplify the model the rotor and stator reluctances, per pole, were combined

Table 7.4. *Summary of the changes in ampere turns, flux for pole eleven, UMP and terminal voltage relative to the magnetically symmetric rotor. Measured/simulated results.*

Configuration	ΔAt [%]	$\Delta\Phi_{POLE11}$ [%]	F_{UMP} [N]	ΔU [%]
4.3	4.28	4.4/3.6	118/101	0.51/0.33
9.5	9.50	8.6/7.3	234/223	0.74/0.73
17	17.4	15.0/14.2	378/401	1.4/1.4
30	29.6	25.5/23.9	612/659	2.4/2.4

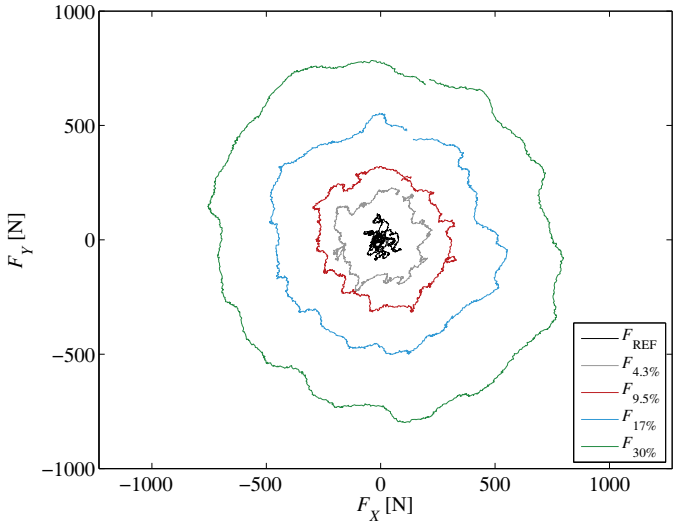

Figure 7.5. The measured force orbits from various degrees of field winding interturn short circuit on pole eleven. The black small orbit in the middle comes from mechanical and magnetic unbalances in the rotor of the experimental generator. Its maximum amplitude is approximately 70 N.

into a single reluctance. The resulting fluxes, shown in figure 7.6 exhibit the same pattern as described above for the flux density measurements. Article IV describes the magnetic circuit in more detail.

7.5 Results not included in the articles

Damper winding circuit parameters

Damper winding resistance and inductance for the configuration with two damper bars and no interpole connector, D13-NC, were determined from the measured damper winding voltage and current.

The stator slot ripple in the measurements was quite pronounced as can be seen in figures 7.7 and 7.8. To avoid the problem of slot ripple the data for both

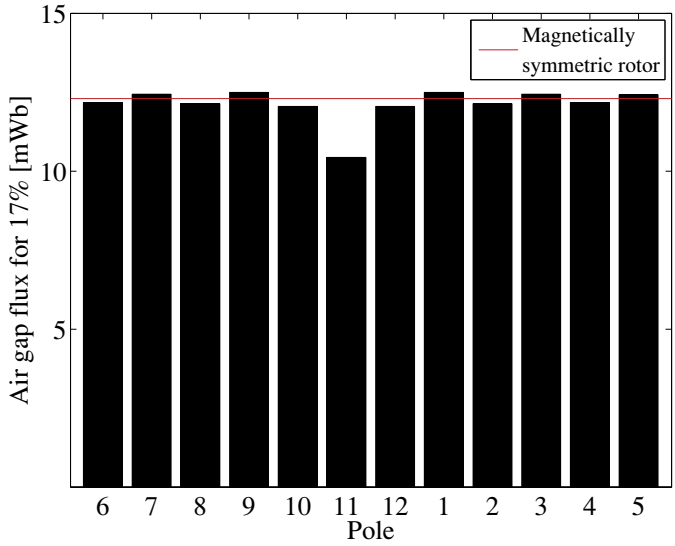

Figure 7.6. The pole flux from the configuration with 17% interturn short circuit on pole eleven calculated the magnetic circuit. The red line represents the pole flux for the rotor without any parallel resistor on pole eleven.

voltage and current was fitted to the function shown in equation 5.4 before the circuit parameters were estimated. The fitted data was then used to find R_D and L_D in

$$U_D = R_D I_D + L_D \frac{dI_D}{dt}. \tag{7.1}$$

where U_D and I_D are the fitted voltage and current. The damper winding resistance, R_D, was found to be 2.3 mΩ. As a comparison, the resistance calculated from material resistivity only was 0.4 mΩ. Contact resistances between the damper bars and the interbar connectors are believed to be the main cause of the difference between the experimental and theoretical values. Regarding the inductance, L_D, some caution should be used in the interpretation of the obtained value of 4 μH. With a measured phase shift between voltage and current of 5.5 degrees, shown in figure 7.9, there is some room for measurement error and at small angles the relationship between measured angle and the inductance is approximately linear. A fit of the measured data, where the slot ripple is prominent, to equation 7.1 results in the same R_D and an inductance of 3.2 μH. The latter value for L_D is most likely closer to the true value due to the larger effect of the inductance at the slot frequencies.

The impact of the inductance is quite small at the mechanical frequency, 8.3 Hz, but at the slot ripple frequency of 900 Hz the effect is large as can be seen from the difference in the relative slot ripple amplitude in the voltage in figure 7.7 and the current in figure 7.8.

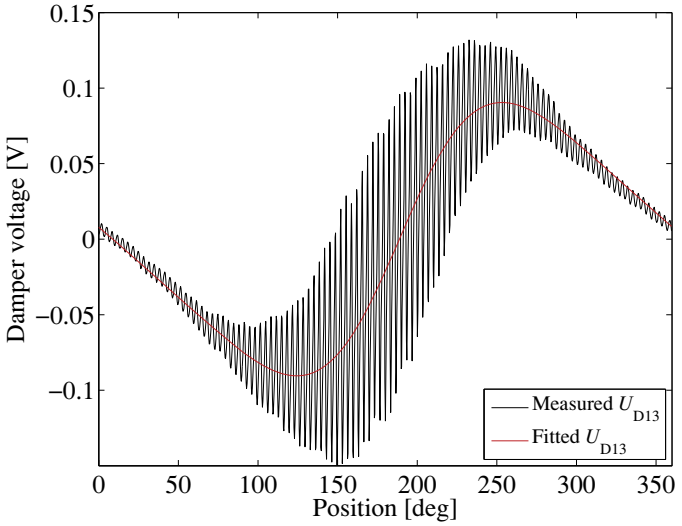

Figure 7.7. The measured and fitted damper voltage for the configuration with two damper bars and no interpole connectors. The stator slot ripple in the damper voltage is more prominent in the part of the revolution where the air gap is small.

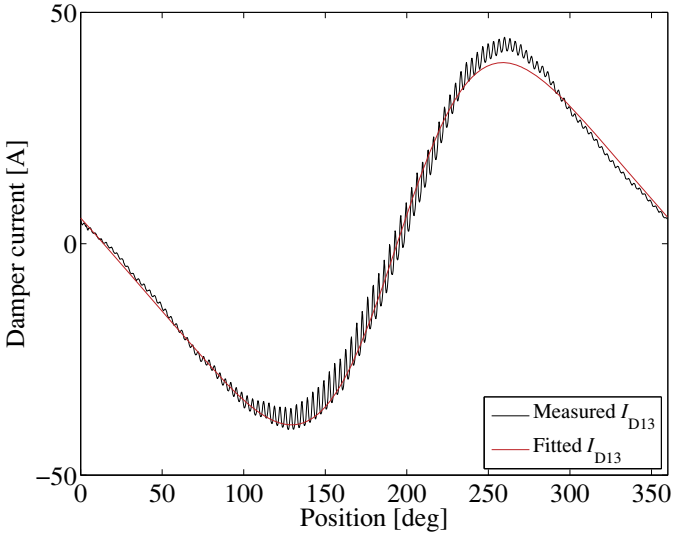

Figure 7.8. The measured and fitted damper current for the configuration with two damper bars and no interpole connectors.

Flux density and damper voltage measurement verification

As a verification of the measurement equipment the expected induced damper voltage calculated from the measured variation in air gap flux density was compared to the actual damper voltage. To avoid the noise of the stator slot

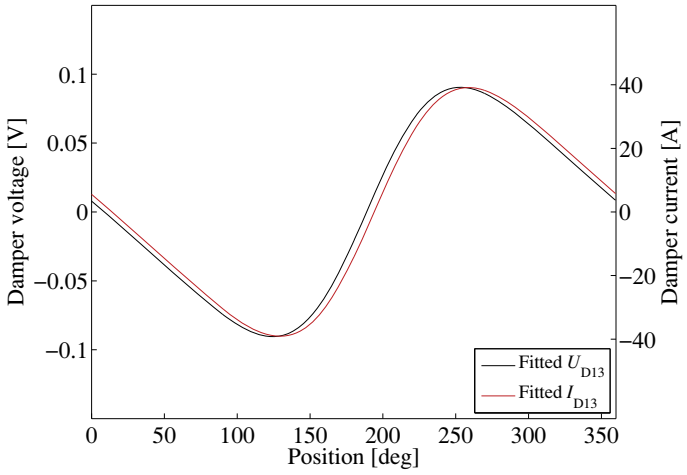

Figure 7.9. The fitted damper voltage and current for the configuration with two damper bars and no interpole connectors. Note the different scales on the two y axes.

ripple the flux density was fitted to equation (3.11) before the expected induced voltage was calculated. Figure 7.10 contains the graphs of the measured and fitted rotor flux density. One thing worth noticing in the figure is how pronounced the stator slot ripple is near where the air gap is at its shortest, at 180 degrees, compared to on the opposite side of the generator. From the rotor flux the damper voltage the calculated as according to equation (5.4). The resulting calculated damper voltage together with its measured value can be seen in figure 7.11.

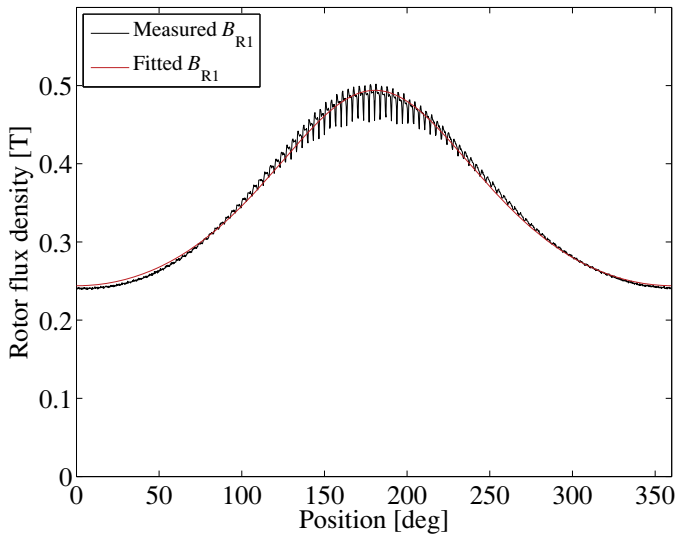

Figure 7.10. Sensor one shown in 6.1 was used to measure the air gap flux density in front of one of the poles. Here both the measured flux density, containing significant slot ripple in the small air gap, and its fitted value can be seen.

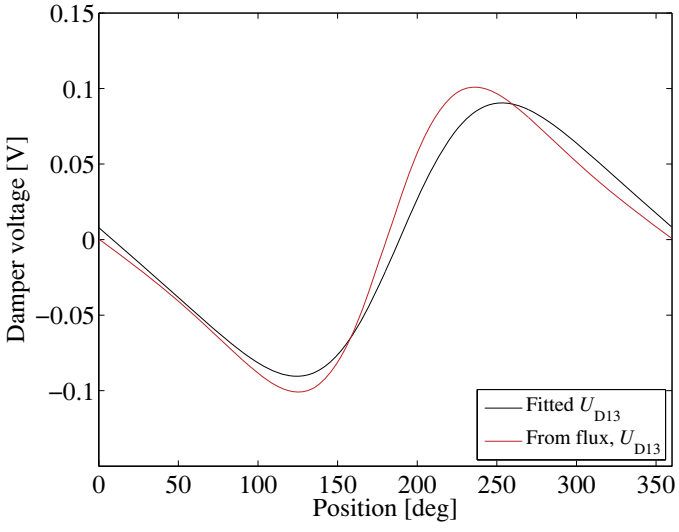

Figure 7.11. The damper voltage calculated from the variation in flux density in the air gap.

8. Summary of articles

In this chapter short summaries of the contents of the articles included in the dissertation are presented. The authors contribution to each article is also specified.

Article I

Design and construction of a synchronous generator test setup

This paper contains a description of the functionality of the test generator setup. Characteristics of the generator as well as the installed measurement equipment are discussed. An initial test of the effect of damper winding configuration on voltage harmonics is included.

The paper was presented by the author, who is the main author of the paper, at The XIX International Conference on Electrical Machines in Rome, Italy, 2010. It was also selected for inclusion in the IEEE Xplore database.

Article II

Reduction of unbalanced magnetic pull in synchronous machines due to parallel circuits

The first experiment on the test generator concerning rotor eccentricity is described in this article. Measurements of the UMP and currents in the parallel circuits have been performed under static eccentricity with the stator winding connected as one circuit or two parallel circuits. Experiments were done at noload conditions. Two numerical studies of the force reduction are also presented, one using a finite element code and one using a permeance model. The reduction of UMP was strongly dependent on the direction of unbalance relative to the line of separation of the stator circuits. Eddy currents induced in the rotor during operation were found to reduce the standstill UMP with more than 20 percent.

The author performed the measurements and the finite element simulations presented and he is the main author of the article.

The article was published in IEEE Transactions on Magnetics, vol. 47(12), pp 4827-4833, December 2011

Article III

Damper winding influence on unbalanced magnetic pull in hydropower generators with rotor eccentricity

Continuous and noncontinuous damper windings resulted in different damper winding currents but their effect on the UMP was found to be very similar. Measurements of the UMP, damper bar currents and air gap flux density were performed on the experimental generator configured with static eccentricity under no-load conditions. Finite element simulations of the different configurations detailing the damper winding induced flux changes are also presented.

The author performed the measurements and simulations presented and he is the main author of the article.

The article was submitted to IEEE Transactions on Magnetics, November 2012

Article IV

Dynamic unbalanced pull from field winding turn short circuits in hydropower generators

The UMP resulting from field winding interturn short circuits is investigated both experimentally and through numerical modelling. Flux density measurements are performed on the experimental generator as well as on a 28 pole production generator. The occurrence of parallel stator branches combined with a field winding short circuit gives rise to circulating stator currents which are analysed. A field winding short circuit in one pole gives rise to an increase in the flux in the other poles with the same polarity. This effect is explained.

The author performed the measurements and simulations presented and he is the main author of the article.

The article was submitted to Electric Power Components and Systems, February 2013

Article V

Standstill frequency response test on a synchronous machine extended with damper bar measurements

Standstill frequency response (SSFR) test data including damper winding measurements for three physically different damper winding configurations is presented. A method to incorporate measured damper bar voltages and currents in the SSFR analysis scheme is proposed. The validity of the generator models identified through the test is substantiated by comparison of the simulated and measured machine response to a drive torque step disturbance.

The author contributed to the measurements performed for the study and the development of the equivalent damper circuit.

Manuscript

9. Svensk sammanfatting

1878 kallade Aristide Bergès vattenkraften för det vita kolet, fr. *la houille blanche*, för att visa på den mängd kraft som fanns lätt tillgänglig i snön och isen i de franska alperna.

Vattenkraftutvinning i industriell skala i Sverige tog sin början 1910 i och med drifttagningen av de fyra första generatorerna i Olidans kraftverk i Göta Älv. Det första större vattenkraftverket i norra Sverige, Porjus, invigdes 1915.

Fram till att kärnkraft började tas i bruk för elproduktion i Sverige under sjuttio- och åttiotalen stod vattenkraften för den överväldigande delen av den elektricitet som producerades. Vattenkraften var och är en avgörande förutsättning för den svenska industrin och välfärden. I dag står vattenkraften för 45 procent, eller 65 TWh, av den elektricitet som används i Sverige.[1]

Även om tekniken är väl utvecklad så finns det ett behov av en ökad förståelse för elektromagnetiska fenomen i synkrongeneratorer för att undvika onödigt slitage, minskad livslängd och haverier. Osäkerhet i elförsörjningen såväl som högre elektricitetspriser, saker som påverkar både industrin och hushållen, kan bli följden av driftproblem inom vattenkraften.

Vid sidan om de ekonomiska konsekvenserna så bör vattnet i våra redan utbyggda älvar av miljöskäl utnyttjas på ett optimalt sätt i väl fungerande vattenkraftverk.

Asymmetriska magnetkrafter uppstår när rotorn i en generator inte är centrerad i statorn eller när det magnetiska flödet i luftgapet av någon annan anledning inte är symmetriskt. Dessa krafter kan förkorta livslängden på generator eller orsaka haveri genom ökat slitage på lager och andra infästningskomponenter för rotorn och statorn. Asymmetriskt luftgapsflöde kan också inducera dämpstavsströmmar och cirkulerande strömmar i statorn vilket leder till resistiva förluster och större värmeutveckling, vilket i sin tur medför ökade ekonomiska förluster och ett ökat termiskt åldrande hos maskinen.

Denna avhandling undersöker i tre studier olika konsekvenser av magnetisk obalans hos synkrongeneratorer.

Arbetet avhandlingen grundas på har utförts vid Avdelningen för elektricitetslära vid Uppsala universitet. Resultat har inhämtats från numerisk analys, analytiska modeller och mätningar på den experimentutrustning som byggts av författaren.

Forskningen som presenteras här är en del i ett Elektraprogram som heter *Utveckling av elektromagnetiska lastmodeller för simulering av interaktionen mellan rotor och stator i vattenkraftgeneratorer.* Elektra finansieras av

[1] Elektricitet utgör en tredjedel av den energi som används i Sverige [1].

ABB, Trafikverket, Svenska Kraftnät och, genom Svensk energi, ett flertal producent- och transmissionsföretag. Elektras syfte är att ”långsiktigt stärka den svenska industrins konkurrenskraft och då i första hand elleverantörer, kraftindustri och tillverkande industri.”

Avhandlingen inleds med en kort beskrivning av hur en synkrongenerator fungerar och hur rotorexcentricitet ger upphov till obalanskrafter. Därefter kommer i kapitel 4 en beskrivning av den finita elementmetod som använts i datorsimuleringarna. Det följande kapitlet beskriver de fyra forskningsområdena parallella kretsar och rotorexcentricitet, dämplinding och rotorexcentricitet, fältlindningskortslutning och karakterisering av synkronmaskiner genom frekvensresponstester. Kapitel 6 är en genomgång av konstruktionsprocessen av experimentgeneratorn samt den mätutrustning som installerats. Avhandlingen avslutas med en resultatdel.

10. Acknowledgements

I, the author, am indebted to Elektra and its member organisations for making this research possible. Sven Jansson should be mentioned for being positive, interested and helpful in every aspect.

Construction of the test generator would not have been possible without the very much appreciated help of Swedish Hydropower Centre, Svenskt vattenkraftcentrum, SVC, and Carl Tryggers stiftelse.

I want to thank Svante Leonsson at GE Hydro who donated the synchronous motor without which the experimental generator could not have been built. Additional help as well as good advice on construction matters was received from Ove L. Andersson at SKF.

The meetings and discussions with the members of the Elektra and SVC steering committee for research in hydropower generators have been a great source of inspiration and advice to me. I am grateful to its members Jan-Olov Aidanpää, Peter Altzar, Per-Olof Andersson, Mats Berg, Christer Bäck, Niklas Dahlbäck, Håkan Hermansson, Anders Holm, Thommy Karlsson and Mats Wahlén for showing interest in my work, all the discussions we have had and, not to forget, the time they have spent travelling to our meetings.

I want to thank Mikael Jonsson together with the rest of the administrative and technical staff at the Department of engineering sciences and the Division of electricity. Without them there would have been no research to write about.

My assistant supervisor, Mats Leijon, should be mentioned for the good atmosphere he has created at the Division of electricity and the group of skilled and kind people he has gathered here.

I am very grateful to my supervisor Urban Lundin for his encourgement, good comments on my writing and keen eye for interesting research topics.

In my daily work the discussions with my friend and colleague Johan Bladh has been of great importance to both my research and to the atmosphere in the office.

My former colleague Martin Ranlöf is worth a special mentioning for the discussions we had, which I learnt a lot from, and for the work he did on the experimental generator.

The rest of the hydropower group with Birger Marcusson, José Pérez-Loya, Linn Saarinen and Per Sundqvist is a wonderful team which it has been great fun to work in.

It has been a pleasure to work and teach with Mikael Bergkvist.

My dear friend Alexander has helped me to have a normal life away from work.

I want to thank my parents and brother for being the best family anyone can have and for putting up with me talking about my research.

Finally I want to thank Ann who decided to join my life as my time as a PhD student was coming to an end and things started to get hectic. The time with you has made everything easy. Thank you.

Bibliography

[1] Swedish Energy Agency. Energy in Sweden - facts and figures 2012, 2013.

[2] M. Ranlöf, R. Perers, and U. Lundin. On permeance modeling of large hydrogenerators with application to voltage harmonics prediction. *IEEE Trans. Energy Convers.*, 25:1179–1186, 2010.

[3] J. H. Walker. *Large Synchronous Machines - Design Manufacture, and Operation*. Clarendon press, Oxford, 1981.

[4] A. Nicolet, F. Delince, N. Bamps, A. Genon, and W. Legros. A coupling between electric circuits and 2d magnetic field modeling. *Magnetics, IEEE Transactions on*, 29(2):1697–1700, Mar 1993.

[5] G. Bedrosian. A new method for coupling finite element field solutions with external circuits and kinematics. *Magnetics, IEEE Transactions on*, 29(2):1664–1668, Mar 1993.

[6] W.M. Arshad, H. Lendenmann, and H. Persson. End-winding inductances of mva machines through fem computations and iec-specified measurements. *Industry Applications, IEEE Transactions on*, 44(6):1693–1700, Nov.-dec.

[7] U. Lundin and A. Wolfbrandt. Method for modelling time-dependent nonuniform rotor/stator configurations in electrical machines. *Magnetics, IEEE Transactions on*, 45:2976–2980, 2009.

[8] Antero Arkkio. *Analysis of induction motors based on the numerical solution of the magnetic field and circuit equiations*. PhD thesis, Helsinki University of Technology, Laboratory of Electromechanics, Helsinki, Finland, 1987.

[9] S. Keller, M.T. Xuan, J.-J. Simond, and A. Schwery. Large low-speed hydro-generators – unbalanced magnetic pulls and additional damper losses in eccentricity conditions. *Electric Power Applications, IET*, 1(5):657–664, 2007.

[10] IEEE Std 115-2009. IEEE Guide: Test procedures for synchronous machines, Part I - Acceptance and performance testing, Part II - Test procedures and parameter determination for dynamic analysis, 2010.

[11] S Lagerkvist. *Kompendium i konstruktiv elktromaskinlära, Del II synkronmaski-nen*. Chalmers, Göteborg, 1963.

[12] A. Elez, B. Tomicic, and A. Colak. The comparison of magnetic values obtained from hall probes and measuring coils in synchronous generators. In *Electrical Machines, 2008. ICEM 2008. 18th International Conference on*, pages 1–4, sept. 2008.

Acta Universitatis Upsaliensis

Digital Comprehensive Summaries of Uppsala Dissertations from the Faculty of Science and Technology 1029

Editor: The Dean of the Faculty of Science and Technology

A doctoral dissertation from the Faculty of Science and Technology, Uppsala University, is usually a summary of a number of papers. A few copies of the complete dissertation are kept at major Swedish research libraries, while the summary alone is distributed internationally through the series Digital Comprehensive Summaries of Uppsala Dissertations from the Faculty of Science and Technology.

Distribution: publications.uu.se
urn:nbn:se:uu:diva-196490

ACTA
UNIVERSITATIS
UPSALIENSIS
UPPSALA
2013